

Iterative Framework of Machine-Learning Based Turbulence Modeling for Reynolds-Averaged Navier-Stokes Simulations

Weishuo Liu^{1,*} and Jian Fang^{2,†}

¹School of Energy and Power Engineering, Beihang University

37 Xueyuan Road, Haidian District, Beijing 100191, China

*²Scientific Computing Department, Science and Technology Facilities Council,
Daresbury Laboratory, Keckwick Lane, Daresbury, Warrington, WA4 4AD, UK*

(Dated: September 20, 2022)

Abstract

A framework of machine-learning (ML) based turbulence modeling for Reynolds-averaged Navier-Stokes (RANS) equations is developed to close the Reynolds stress term in the RANS equations. Several principles for turbulence modeling using ML techniques are discussed, including the effectiveness of the closure term and sufficiency of input variables for a ML model. An iterative computational process is implemented between the ML model and the RANS solver to ensure the convergence of simulations to the training data, and the transport equations of a conventional turbulence model are also solved to assist the ML modeling. A cross-case training strategy is adopted with the data from direct-numerical simulations of turbulent channel flows at different Reynolds numbers, and the solver is able to predict both the mean flow field and turbulent variables correctly within the training range. A further test in a flow over periodic hills also shows an improved result, indicating a promising prediction capability of the developed model even if the model is trained only with the data of channel flows.

I. INTRODUCTION

The Reynolds-averaged NavierStokes (RANS) equations has been widely used in fluid engineering for decades, and will continue to play an important role in the foreseeable future [1, 2]. Only the mean flow is resolved in the RANS equations, and therefore, the computational cost is much lower than the eddy-resolved simulations. However, the averaging of the N-S equations creates a new Reynolds stress term accounting for the effect of turbulent fluctuations on the mean flow motion and brings a closure problem. Over a hundred years, countless efforts have been devoted to the closure problem and large number of various turbulence models have been developed [3–10]. However, the progress of the closure problem, including the application of turbulence models in computation fluid dynamics (CFD), is still far from satisfactory, and the turbulence model is still the major source of uncertainty of RANS simulations.

Traditionally, a turbulence model is developed based on some simplified hypothesis and approximations (e.g. the Boussinesq hypothesis, the gradient-diffusion hypothesis) summa-

* liuweishuo@buaa.edu.cn

† Corresponding author: jian.fang@stfc.ac.uk

rized from a class of baseline flows, construction of the transport equations of turbulence quantities (e.g. turbulence kinetic energy, turbulence dissipation rate, eddy-viscosity), and tunable parameters. However, the assessment of Kline et al. in 1982 [11] has indicated that none of the turbulence models available in 1980s could give good engineering accuracy in complex flows. Although, some new turbulence models have been developed since 1980s, the conclusion of Kline et al. [11] still holds according to a series of more recent assessments [12–14]. It means that the traditional way of turbulence modeling has reached its limit.

Recently, machine learning (ML) technique, as an efficient tool to deal with complex and high-dimensional input-output relations [15], sheds lights to the RANS closure problem. Latest studies have proved the feasibility of the integration between turbulence models and machine learning algorithms [16, 17] utilizing the data from high-fidelity (HF) simulations.

Generally speaking, a turbulence model is of a combination of transport equations and an algebraic constitutive law to calculate the Reynolds stress (RS) tensor [8, 18], such as those widely used two-equation models [4–6, 9, 10]. Therefore, such two aspects were highly focused by the researchers who were trying to use ML techniques in turbulence modeling. In terms of transport equations, Parish & Duraisamy [19] and Holland et al. [20] developed a field inversion technique to find the spatial distribution of ML target variables. The same strategy combined with a ML technique such as the artificial neural network (ANN) was used to construct a functional form of correction coefficient in the turbulence transport equations. The methodologies was applied and tested in the $S - A$ model [21–23] and the transitional $k - \omega$ model [22, 24]. As for the constitutive law, Ling et al. [25] firstly introduced a specified structure neural network based on the general effective-viscosity hypothesis proposed by Pope [26], and the Galilean invariance is maintained in the tensorial form of the constitutive function [27]. Wang et al. [28] and Wu et al. [29] extended the constitutive expression to four independent tensors and predicted the discrepancy of the RS tensor compared with the results of traditional models, and the random forest algorithm was adopted to select important features within the regression process. Both the method of Ling [25] and the method of Wang et al. [28] and Wu et al. [29] have achieved better results than traditional turbulence models in anisotropic flows, however, the convergence of the iteration between the ML model and the CFD solver were not shown. Similarly, Weatheritt & Sandberg [30, 31] utilized an gene expression programming to find an optimal analytical formula in a tree-based form of expression for each coefficient in an algebraic Reynolds stress model,

leading a novel direction in the parametric modeling method. Favorable algebraic expressions were respectively found for separated flows [30] and duct flows [31], and the application of their model trained with data from low-pressure turbine wake flow showed an improvement compared to linear models [32].

To sum up, the existing studies in the ML based turbulence modeling have managed to reproduce the mean flow of the HF simulations used to construct the ML model, and give favorable predictions of cases sharing a relatively strict physical and geometrical similarity with the training case. However, the obstacle lies in an absence of cross-case training, which would allow the training database to be extensible for cases containing different flow physics for various application scenarios. Also, the convergence of non-parametric models in constructing the constitutive law is still a challenge.

In the present study, we propose a iterative computational framework for the ML based turbulence modeling, aiming at a cross-case data-wise interpolation and the convergence of simulations. The paper is organized as follows. Section II introduces two significant principles of integrating a ML technique into a RANS solver. In Sec. III, we put forward the iterative framework utilizing a traditional turbulence model and the relevant numerical platform. Simulation results are shown in Sec. IV and conclusions are addressed in Sec. V.

II. PRINCIPLES APPLYING ML TECHNIQUE TO TURBULENCE MODELS

In this section, two significant topics are discussed based on previous research and data analysis in a turbulent channel flow. They are also the two most significant problems in the ML based turbulence modeling. Moreover, the iterative ML-CFD framework in this paper is developed based on the following discussion.

A. Effectiveness of the RANS Closure Term

The equations for averaged momentum for incompressible flows can be written in Einstein notation in Cartesian coordinates as:

$$\frac{\partial u_i}{\partial t} + \frac{\partial (u_i u_j)}{\partial x_j} = -\frac{1}{\rho} \frac{\partial p}{\partial x_i} + \frac{\partial}{\partial x_j} \left(\nu \frac{\partial u_i}{\partial x_j} - \overline{u'_i u'_j} \right) + f_i \quad (1)$$

where the term $\tau_{ij} = -\overline{u'_i u'_j}$ is the unclosed Reynolds stress (RS) term due to the averaging operation, u_i is mean velocity component, u'_i is the fluctuate velocity component, p is the

pressure and ν is the molecular velocity.

It can be seen from Eq. (1) that the form of the RANS equations is basically the N-S equations with a correction term (i.e. the Reynolds stress). In principle, as long as a correct Reynolds stress is given, the RANS equations should give a correct prediction of mean flow, and therefore, a turbulence model should aim at narrowing the gap between the modeled RS tensor and the correct RS tensor. However, Wu, et al. [33] have reported that a correct priori estimation of RS tensor doesn't naturally guarantee a correct posterior solution in a prediction case. The RANS equations would be ill-conditioned when the Reynolds stress tensor in the momentum equations is directly extracted from a direct-numerical simulation (DNS), which means the solution is sensitive to the statistical error of the source term. Especially for a flow under a high Reynolds number ($Re_\tau = 5200$), small errors in Reynolds stress will be propagated into a large difference for over 35% in mean velocity [34]. And the mean flows of RANS simulations using similar RS sources could differ vastly from each other [33].

To overcome the sensitive dependence of the RANS equations on the statistical errors of the RS term, Wu, et al. [33] proposed to decompose the RS tensor into a linear part and a nonlinear part, as shown in Eq. (2). It was also proved by Wu et al. [33] that the eddy-viscosity defined by Eq. (3) can improve the stability of the momentum equation.

$$\boldsymbol{\tau} = -2\nu_t \boldsymbol{S} + \boldsymbol{\tau}^\perp \quad (2)$$

$$\nu_t = \frac{\|\tau_{ij} S_{ij}\|}{2\|S_{ij} S_{ij}\|} \quad (3)$$

In Eq. (2) \boldsymbol{S} is the mean strain rate defined as:

$$S_{ij} = \frac{1}{2} \left(\frac{\partial u_i}{\partial x_j} + \frac{\partial u_j}{\partial x_i} \right)$$

and $\boldsymbol{\tau}^\perp$ is the nonlinear part of RS tensor. Note in this paper, all the bold symbols (e.g. \boldsymbol{S}) denotes the form of tensor or vector, and the regular symbols with index (e.g. S_{ij}) are the index form of tensor or vector.

In the present study, the RS term in the RANS equations is expressed in the form of Eq. (2) and (3). It should be mentioned that in a channel flow with two homogeneous directions, the mean flow variables are one-dimensional functions in the wall-normal direction, and only the τ_{12} component of the RS tensor (i.e. the Reynolds shear stress) has a contribution to the mean momentum equation Eq. (1). In such a case, the nonlinear part of RS tensor

makes no contribution to the momentum equation and only the eddy-viscosity, ν_t is need to be modeled.

B. Sufficiency of Independent Variables

Turbulence models aim at building a connection between the closure term and mean flow field. The basic assumption of algebraic stress model [8, 35] has been inherited and widely adopted in previous studies, as presented in Eq. (4).

$$\begin{aligned} \mathbf{b} &= \mathbf{f}(\hat{\mathbf{S}}, \hat{\mathbf{\Omega}}) \\ \mathbf{b} &= \sum_{n=1}^{10} G^{(n)}(\lambda_1, \dots, \lambda_5) \mathbf{T}^{(n)} \end{aligned} \quad (4)$$

$$\mathbf{T}^{(i)} = \begin{cases} \mathbf{T}^{(1)} = \hat{\mathbf{S}} & \mathbf{T}^{(6)} = \hat{\mathbf{\Omega}}\hat{\mathbf{S}}^2 + \hat{\mathbf{S}}^2\hat{\mathbf{\Omega}} - 2/3\mathbf{I} \cdot \text{tr}(\hat{\mathbf{S}}\hat{\mathbf{\Omega}}^2) \\ \mathbf{T}^{(2)} = \hat{\mathbf{S}}\hat{\mathbf{\Omega}} - \hat{\mathbf{\Omega}}\hat{\mathbf{S}} & \mathbf{T}^{(7)} = \hat{\mathbf{\Omega}}\hat{\mathbf{S}}\hat{\mathbf{\Omega}}^2 - \hat{\mathbf{\Omega}}^2\hat{\mathbf{S}}\hat{\mathbf{\Omega}} \\ \mathbf{T}^{(3)} = \hat{\mathbf{S}}^2 - 1/3\mathbf{I} \cdot \text{tr}(\hat{\mathbf{S}}^2) & \mathbf{T}^{(8)} = \hat{\mathbf{S}}\hat{\mathbf{\Omega}}\hat{\mathbf{S}}^2 - \hat{\mathbf{S}}^2\hat{\mathbf{\Omega}}\hat{\mathbf{S}} \\ \mathbf{T}^{(4)} = \hat{\mathbf{\Omega}}^2 - 1/3\mathbf{I} \cdot \text{tr}(\hat{\mathbf{\Omega}}^2) & \mathbf{T}^{(9)} = \hat{\mathbf{\Omega}}^2\hat{\mathbf{S}}^2 + \hat{\mathbf{S}}^2\hat{\mathbf{\Omega}}^2 - 2/3\mathbf{I} \cdot \text{tr}(\hat{\mathbf{S}}^2\hat{\mathbf{\Omega}}^2) \\ \mathbf{T}^{(5)} = \hat{\mathbf{\Omega}}\hat{\mathbf{S}}^2 - \hat{\mathbf{S}}^2\hat{\mathbf{\Omega}} & \mathbf{T}^{(10)} = \hat{\mathbf{\Omega}}\hat{\mathbf{S}}^2\hat{\mathbf{\Omega}}^2 - \hat{\mathbf{\Omega}}^2\hat{\mathbf{S}}^2\hat{\mathbf{\Omega}} \end{cases}$$

$$\lambda_1 = \text{tr}(\mathbf{S}^2), \lambda_2 = \text{tr}(\mathbf{\Omega}^2), \lambda_3 = \text{tr}(\mathbf{S}^3), \lambda_4 = \text{tr}(\mathbf{\Omega}^2\mathbf{S}), \lambda_5 = \text{tr}(\mathbf{\Omega}^2\mathbf{S}^2)$$

where \mathbf{b} is the deviatoric tensor of Reynold Stress normalized by turbulence kinetic energy $k = \overline{u'_i u'_i}$, defined in Eq. (5), $\hat{\mathbf{S}}$ and $\hat{\mathbf{\Omega}}$ are the normalized strain and rotate tensor defined in Eq. (6), and ϵ shown in Eq. (6) is the dissipation rate of turbulence kinetic energy. $G^{(n)}$ are the combination coefficients of tensor base $\mathbf{T}^{(n)}$, which are functions of tensor invariances λ_i .

$$b_{ij} = \overline{u'_i u'_j} / k - 2/3 \delta_{ij} \quad (5)$$

$$\begin{aligned} \hat{S}_{ij} &= \frac{1}{2} \frac{k}{\epsilon} \left(\frac{\partial u_i}{\partial x_j} + \frac{\partial u_j}{\partial x_i} \right) \\ \hat{\Omega}_{ij} &= \frac{1}{2} \frac{k}{\epsilon} \left(\frac{\partial u_i}{\partial x_j} - \frac{\partial u_j}{\partial x_i} \right) \end{aligned} \quad (6)$$

One advantage of this formula is that \mathbf{b} , \mathbf{S} and $\mathbf{\Omega}$ in above equations are all Galilean invariant. However, this form assumes an equilibrium state of turbulence [35], which means the Reynold Stress is only related to the local velocity gradient. While in a non-equilibrium turbulent flow, more information is needed to calibrate the local non-equilibrium state to obtain a more accurate estimation of local flow.

The basic assumptions of the algebraic stress model are first analyzed in a turbulent channel flow using the DNS data of Abe et al. [36] at $Re_\tau = 180$. In a channel flow, only the b_{12} component of the Reynolds stress has a contribution to the mean flow and the only nonzero component of the strain-rate tensor is S_{12} . The relation between b_{12} and S_{12} in the channel flow is plotted in Fig. 1.

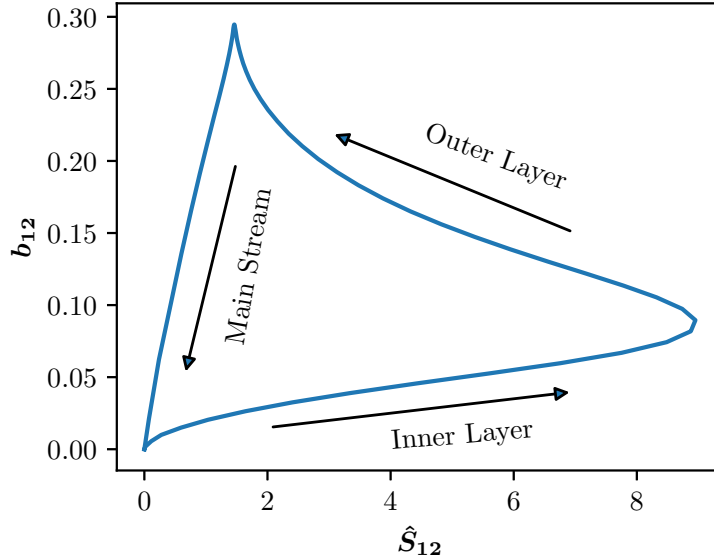


FIG. 1. Constitutive relation in turbulent channel flow

It can be seen from Fig. 1 that the b_{12} term is actually a double-valued function of S_{12} , which indicates that we need to introduce more independent variables to construct a single-valued functional relationship. Based on the theory of the tensor analysis and matrix polynomials [37–39], the form of the function could be extended by adding any number of Galilean invariant scalars \tilde{q}_j without changing the tensorial basis. Therefore, more dimensionless scalars as independent variables are introduced to the (4), as shown in Eq. (7), and the coefficient of each tensorial base becomes a function of λ_i and \tilde{q}_j , shown in Eq. (8).

$$\mathbf{b} = \mathbf{f}(\hat{\mathbf{S}}, \hat{\mathbf{\Omega}}, \tilde{q}_j) \quad (7)$$

$$G^{(n)} = g^{(n)}(\lambda_i, \tilde{q}_j) \quad (8)$$

In this way, the double-valued problem can be overcome and the Galilean invariance is still preserved. Note that the first coefficient $G^{(1)}$ is related to the linear part of the RS tensor, and by combining Eq. (2), Eq. (4) and Eq. (5), one could get:

$$\nu_t^* = \frac{\nu_t}{\nu} = G^{(1)} \frac{k^2}{\nu\epsilon} = G^{(1)} m^* = f(\lambda_i, \tilde{q}_j, m^*) \quad (9)$$

In practice, velocity-derived quantities could cause a numerical instability in iteration process, as reported by Durieux [40]. So, λ_i is not used in constructing the function. Furthermore, $m^* = k^2/(\nu\epsilon)$ is also a Galilean invariance scalar and added into $\{q_n\} = \{\tilde{q}_j, m^*\}$. Therefore, the final functional form for the ML task can be written as:

$$\nu_t^* = f(q_n) \quad (10)$$

where q_n must include m^* .

Based on the two aspects discussed above, on the one hand, the closure term defined in a diffusional form to introduce eddy-viscosity is needed to overcome the ill-conditioned problem of RANS equation. Therefore, the consistency of priori and posterior performance can be ensured. On the other hand, the previously accepted general effective viscosity hypothesis [26] shows its limits even in the simplest turbulent flow case for not introducing enough independent variables. Therefore, the set of independent variables is extended to sufficiently define the output value.

III. ML-RANS FRAMEWORK & NUMERICAL PLATFORM

In this part, we propose an iterative ML-RANS framework based on the discussion in Sec.II. **A basic requirement should be satisfied:** if the HF statistical averaged velocity field is used as the initial field, the solution obtained after one iteration step should not deviate significantly from the initial field. So, this study aims at a from- \mathbf{u}_{DNS} -to- \mathbf{u}_{DNS} close-loop computation framework.

For the construction of input variables for the ML model, the local turbulence quantities need to be estimated. We address the equations of a traditional turbulence model to assist the ML modeling for two major reasons. First of all, a classic turbulence model can give a favorable estimation of turbulence quantities, providing the necessary normalization

factors for mean flow quantities needed by Eq. (6). The second reason is that the estimated turbulence quantities would help to create more independent non-dimensional fields, ensuring the sufficiency of the input variables for ML models. In this present study, the $k - \omega$ SST model (2003) [6] is chosen for its numerical stability and integrability in near-wall region. Thus, the dissipation rate of turbulence kinetic energy, ϵ , is substitute by the product of k and ω . The necessary dimonsionless scalar m^* in q_n becomes:

$$m^* = k/(\nu\omega)$$

Based on the discussion to achieve the requirement above, the calculation process of the ML-RANS framework is designed as follows and shown Fig. 2:

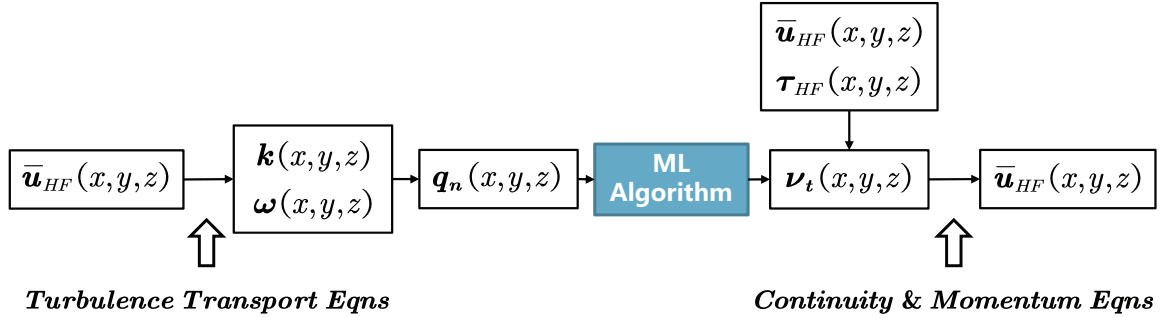


FIG. 2. Illustration of the computational process within one iteration step

1. The accurate mean flow field is provided from a HF simulation, based on which the transport equations of k and ω of the $k - \omega$ SST turbulence model are solved to get the turbulent quantities.
2. The input features for the ML model, $\{q_n\}$, are thus constructed by the combination of mean velocity and turbulent quantities.
3. The learning target (i.e. the accurate eddy-viscosity) for the ML model is obtained by calculating ν_t using Eq. (3) from the data of the HF simulation.
4. After the training processing of the ML model, the mapping between accurate mean flow field and accurate eddy-viscosity can be established in the ML model. The RANS simulation based on the accurate eddy-viscosity and the accurate initial field is ensured to reproduce the accurate mean flow field based on the procedure we adopted in the Sec.II-A. Therefore, the proposed calculation process can ensure the RANS simulation to reproduce the mean flow field of the HF data used to train the mode, within one iteration step.

Based on the design of single-step computation, the current ML-RANS framework is constructed with two major phases, the training phase and the predicting phase, as sketched

in Fig. 3.

In the training phase, the turbulent quantities (e.g. the turbulence kinetic energy k and the specific rate of dissipation ω) are estimated by solving the transport equations of a conventional turbulence model (e.g. $k - \omega$ SST turbulence model) based on the mean flow field of the training data. $\{q_n\}$ is then calculated as the input features of the ML model. The output of the ML model is the eddy-viscosity, ν_t , and the eddy-viscosity from the training data using Eq. (3) is used as the learning target. The training process is finished when the error between outputted ν_t from the ML model and the target ν_t achieves a certain tolerance. By the end of the training phase, the mapping between accurate mean flow field and accurate eddy-viscosity is established in the ML model.

In the predicting phase, the ML model acquired from the above training phase is loaded to a CFD solver. At each iteration step, the ML model receives mean flow field and turbulent quantities from the CFD solver, and outputs the eddy-viscosity. The CFD solver, on the other hand, receives the eddy-viscosity from the ML model, solves the RANS equations and transport equations of a traditional turbulence model respectively to get the mean flow field and turbulent quantities, and passes them to the ML model. The iterative loop keeps going until the residuals converge to a certain tolerance. (see Fig. 3).

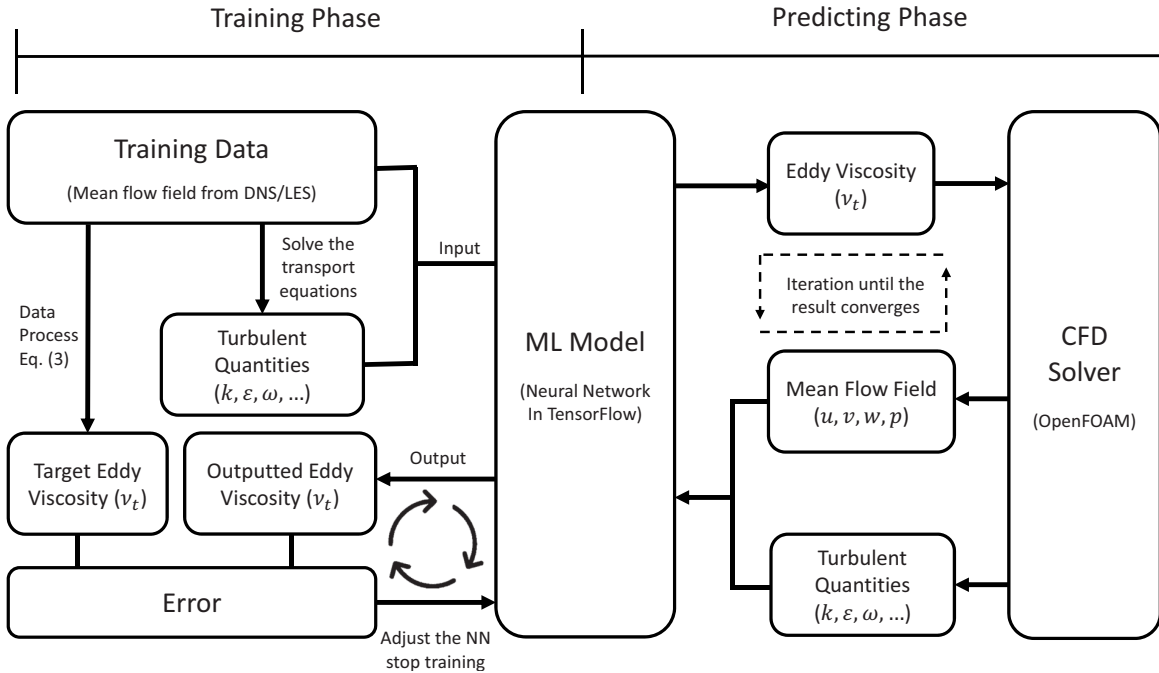


FIG. 3. A comprehensive framework of the ML based turbulence modeling

As for the numerical platform, many ML frameworks have been developed since 2010s [41–44]. Among them, the Tensorflow (TF) [41] library has an abundant Application Programming Interface (API) support in major programming languages. Its computational efficiency is influenced little by the adopted programming language owing to graph-defined properties, and users just need to define the computational operations through the API. Besides, the Tensorflow has the largest user community among open-source ML frameworks. Based on the above reasons, the Tensorflow is selected as the ML library in the present study. For the RANS solver, we chose OpenFOAM [45] for its well encapsulated differential operators, abundant linear solvers, and the user friendliness to build and solve PDE system. Also, OpenFOAM is being extensively used in the CFD community.

IV. RESULTS AND DISCUSSION

The ML model is trained in planar turbulent channel flows from a low Reynolds number to a moderate Reynolds number. Afterwards, the ML-RANS solver is tested in turbulent channel flows, and further extended to a periodic hill flow [46] to evaluate the robustness of the solver.

TABLE I. List of training dataset and testing dataset

Training Phase		Predicting Phase	
Training set	Validation set	Test case	
Planar channel flow [36]	Planar channel flow [47]	Planar channel flow	Flow over periodic hills
$Re_\tau = 180^a$		$Re_\tau = Re_\tau^{train}, Re_\tau^{valid}$	
$Re_\tau = 395$	$Re_\tau = 587.1$	$Re_\tau = 180, 230, \dots, 630$	$Re_h = 1400^b$
$Re_\tau = 640$			

^a Re_τ is the Reynolds number based on the mean wall friction velocity and the half-height of a channel.

^b Re_h is the Reynolds number based on the bulk velocity and the height of the hill.

The DNS data from Abe et al. [36] and Kim et al. [47] (known as KMM database) are used as the training and validation dataset respectively. The training data is used by the optimization algorithms to adjust weights in ANN whereas the validation data is used for adjusting hyperparameters, monitoring and controlling the training process. The DNS of

periodic hill flow at a low-Reynolds number conducted by us is taken as the extension test case. Details of dataset are given in Table. I.

A. Training Phase

The artificial neural network is adopted as the machine learning approach in the present paper. There are six raw input variables for the ANN, q_1 - q_6 as listed in Table 2. In practice, by accounting the range of each input variables, the actual non-dimensional inputs with range adjusted are defined in the last column of Table 2.

TABLE II. Non-dimensional input features for artificial neural network (ANN)

Variable	Description	Definition	Normalization	Actual input
q_1	Turbulence intensity	k	$\frac{1}{2}U_i U_i$	$\frac{25k}{25k + 0.5U_i U_i}$
q_2	Normalize factor m^*	$\frac{k}{\nu\omega}$	Not applicable ^c	$\frac{k}{50\nu\omega}$
q_3	Local Reynolds number	$\frac{\sqrt{k}d_*}{\nu}$	Not applicable	$\frac{\sqrt{k}d}{50\nu}$
q_4	Cross diffusion of k and ω	$\frac{\partial k}{\partial x_i} \frac{\partial \omega}{\partial x_i}$	ω^3	$10 \left(\frac{1 + 680\chi_k^2}{1 + 400\chi_k^2} - 1 \right)^{**}$
q_5	Variables in SST model to characterize viscous sublayer	$\frac{\sqrt{k}}{\omega d}$	Not applicable	$\frac{5\sqrt{k}}{\omega d}$
q_6	and turbulent region	$\frac{\nu}{\omega d^2}$	Not applicable	$\frac{200\nu}{\omega d^2}$

^c Not applicable means the normalization is not necessary.

* d is the distance to the wall.

$$^{**} \chi_k = \max \left(\frac{1}{\omega^3} \frac{\partial k}{\partial x_i} \frac{\partial \omega}{\partial x_i}, 0 \right)$$

The profiles of the input variables in channel flows are shown in Fig. 4, from which we could observe similar distributions between q_2 and q_3 , and between q_1 and q_6 as well. This indicates the six input variables are redundant for the regression system. The output

variables, based on the discussion in Sec. II, is the eddy-viscosity normalized by molecular viscosity, defined in Eq. (11).

$$\nu_t^* = \nu_t / \nu \quad (11)$$

where ν is the molecular kinematic viscosity.

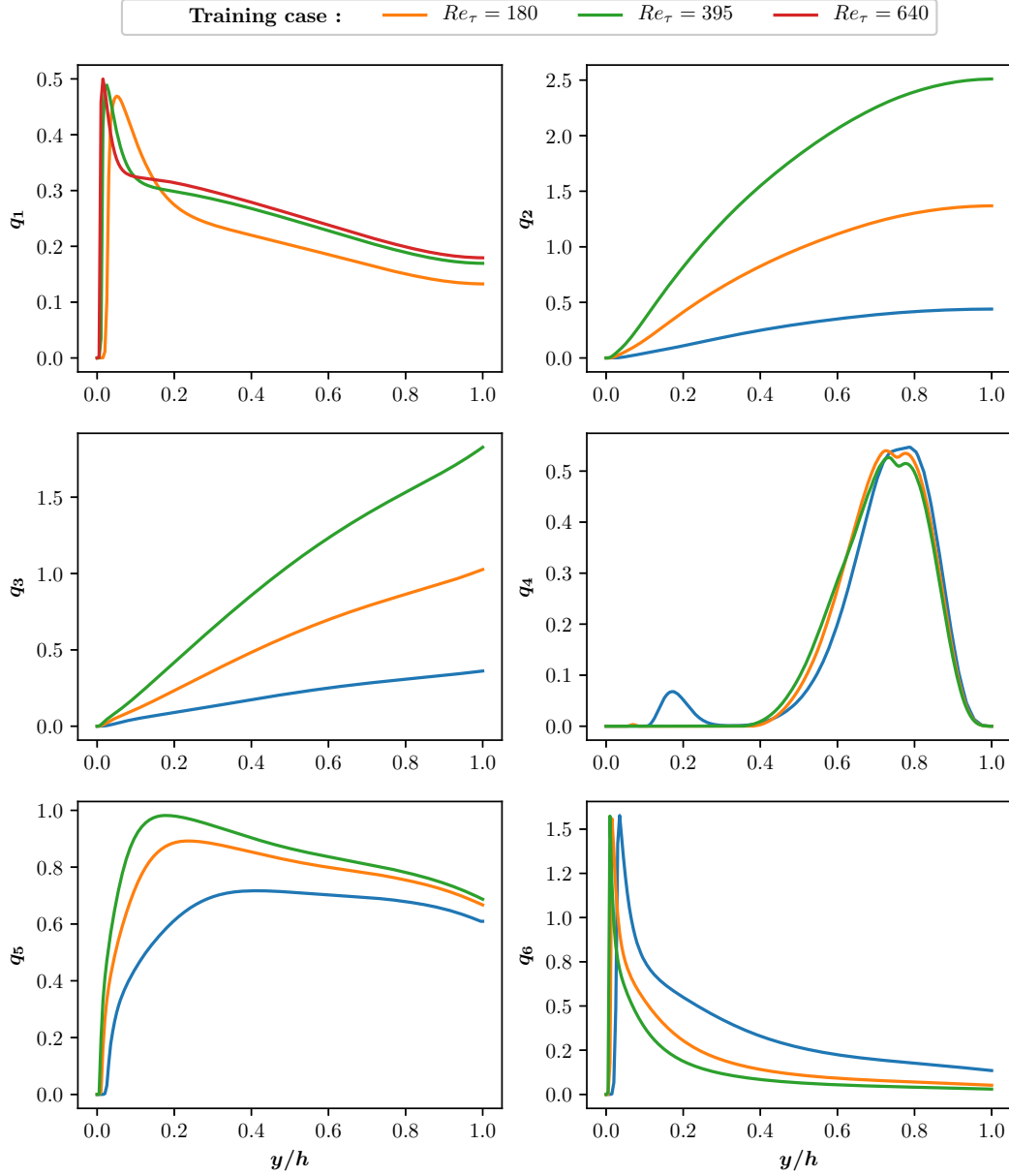


FIG. 4. Profiles of the input variables of the ANN in channel flows

The input and output variables could maintain a rotational invariance, note that the first

input feature contains kinetic energy of mean flow, shifting with a translational transformation of the reference frame. So, a complete Galilean invariance cannot be maintained but the trained model could be applied in any stationary reference frame and the results could be maintained under any rotational transformation system.

In the training process of the ANN, the input and output of the ANN are also calculated using the validation set to monitor the overfitting property during the training process. The total loss of the ANN consists of two different parts as defined in Eq. (12).

$$Loss = \sum_{k=1}^N (f(x_k) - y_k)^2 + \lambda \sum_{i,j}^{m,n} |\omega_{ij}| \quad (12)$$

where N is the number of data point, m and n are the numbers of layers and nodes in the ANN respectively. The optimization is applied to the both parts of the loss. The first part is the mean square error (MSE) from the training data, and the second part is the L1 regularization penalty, minimizing the weight of each layer [48] to achieve a better generalization capability. The evolution of errors during the training process can be seen in Fig. 5.

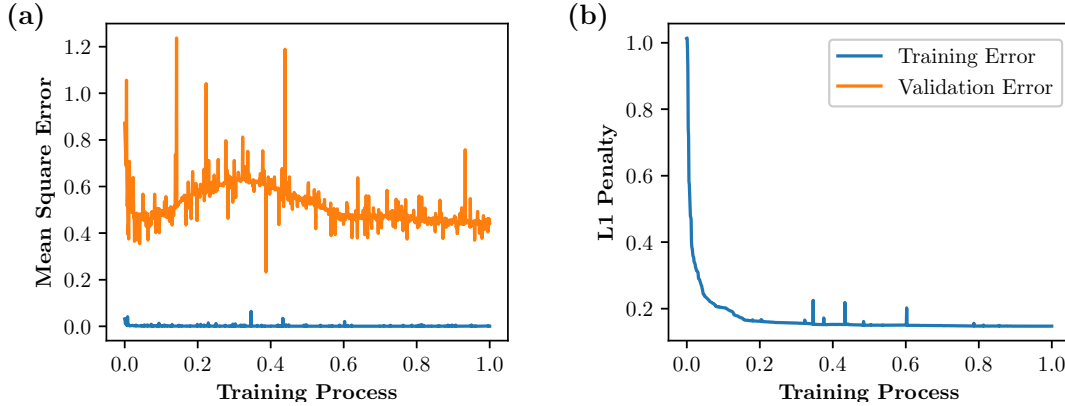


FIG. 5. Losses in the training process. (a): MSE loss (b): L1 penalty term. The x -axis is defined as the ratio of current training step and total training steps.

It should be mentioned that for the current dataset used in the training phase, the quality of the training dataset is better than the validation dataset in terms of the number of samples for averaging and the smoothness of high-order statistics. Consequently, the magnitude of MSE of the validation data is larger than that of the training data. But at the end of the

training, the error of the validation data converges to the lowest level, indicating that ML model is not over-fitted in the training process.

The priori result of the eddy-viscosity is presented in Fig. 6. It can be seen that the eddy-viscosity is perfectly fitted in the training dataset, and a satisfactory result is also achieved in the validation dataset as well.

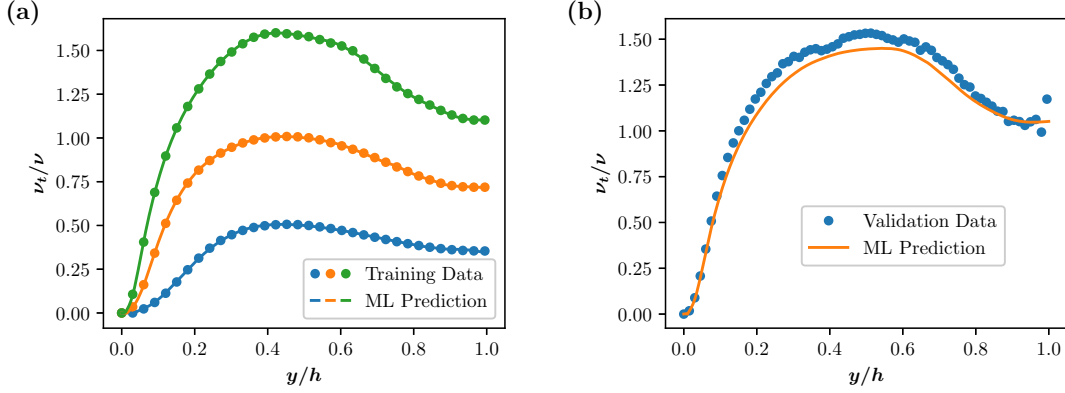


FIG. 6. The eddy-viscosity fitted by the ANN at the end of the training phase. (a): Performance on the training set (b): Performance on the validation set

During the training phase, the overfitting problem is avoided by using a set of noisy data to monitor and control the training process, leading a satisfactory priori prediction on both the training set and the validation set. The details of the hyperparameters in ANN are shown in Table III.

TABLE III. Hyper parameters of a successful training of ANN

Hyper Parameters	Recommend Values
Number of Hidden Layers	3
Number of Nodes per Layer	24
Activation Function	tanh
Optimizer	Adam Optimizer
Learning Rate	0.002
L1 Regularization Coefficient	0.025
Epoch Numbers	1500000

B. Posterior Results in Test Cases

After the ANN being trained, the weights of each layer in the ANN are frozen and the ML model is ready for an online prediction. In the predicating phase, the frozen Tensorflow graph is loaded to the RANS solver to predict eddy-viscosity in each iteration step based on the previous velocity field.

The developed ML model is tested in turbulent channel flows. The two-dimensional Cartesian mesh is used in the simulation and the parameters of the mesh are listed in Table IV. The mesh is uniformly distributed in the streamwise direction and stretched in the wall-normal direction to ensure that the first point off the wall satisfies $y^+|_{wall} \approx 1$ and the maximal mesh resolution $\Delta y_{\max}^+ < 4$. The initial flow field for each test is from a converged RANS simulation using the $k - \omega$ SST model. The residuals are monitored and the simulations stop when the residuals are reduced to a certain level as shown in Fig. 7.

TABLE IV. Mesh details of RANS simulation

Reynolds Number (Re_τ)	Cell Number (I) (flow direction)	Cell Number J (wall normal)
$150 < Re_\tau < 300$	40	168
$300 < Re_\tau < 500$	78	372
$Re_\tau > 300$	128	558

The profiles of mean velocity and mean velocity gradient of the test cases are shown in Fig. 8 and Fig. 9, from which we can confirm that the mean velocity profiles at the same Reynolds number of the training and validation case are simulated perfectly. From the detailed comparison of velocity gradient profiles, we can further confirm that the traditional $k - \omega$ SST model failed to capture the peak and inflection points of the velocity gradient, and the present ML model presents a superior performance in predicating high-order statistics.

The eddy-viscosity profiles are compared in Fig. 10, from which we can see that the $k - \omega$ SST model shows an over-prediction of the eddy-viscosity in the most part of the channel, leading to errors in the mean velocity prediction. The ML model improves greatly the results, and the profiles of eddy-viscosity for all cases agree well with the DNS data. The wiggles on the eddy-viscosity profiles of the KMM database should be due to the inadequacy

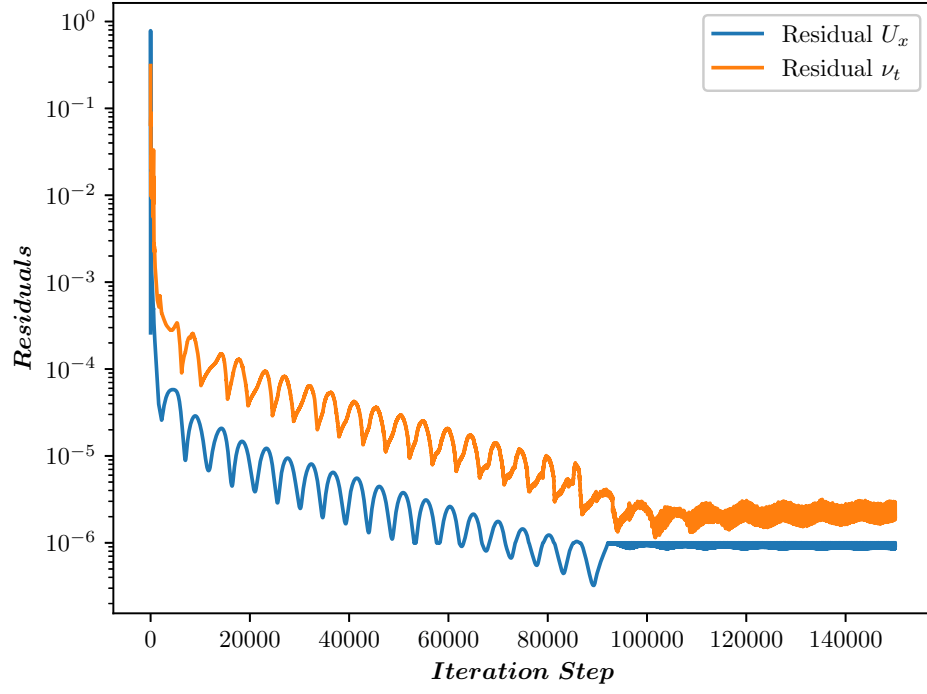


FIG. 7. Evolution of residuals in the simulation of a channel flow.

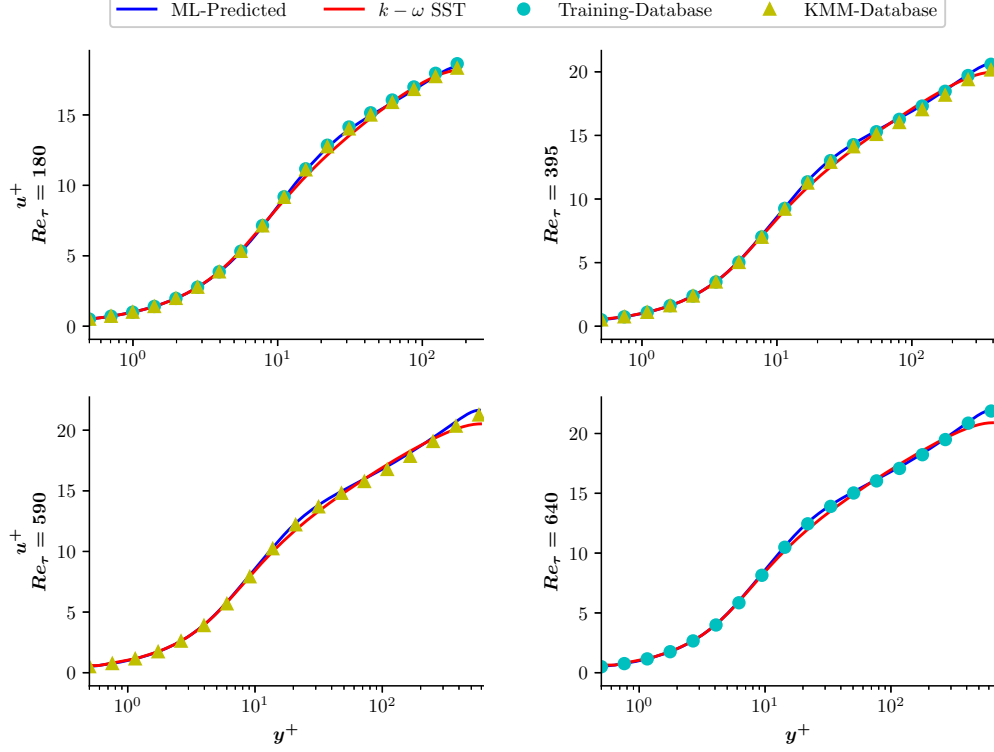


FIG. 8. Comparison of velocity profiles.

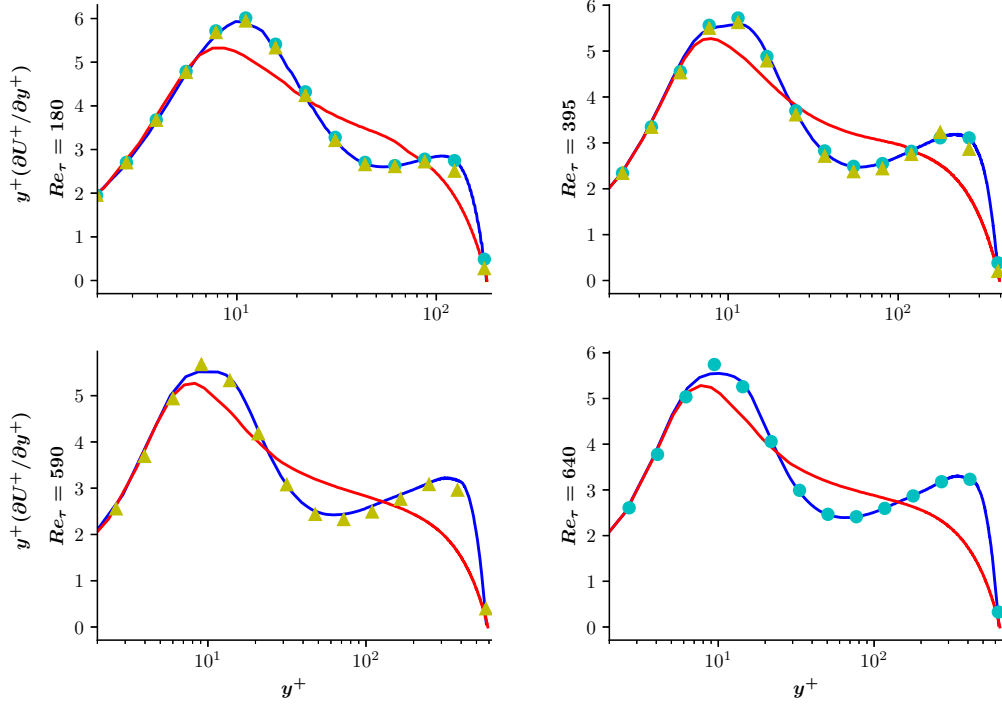


FIG. 9. Comparison of the distributions of $y^+(\partial U^+ / \partial y^+)$.

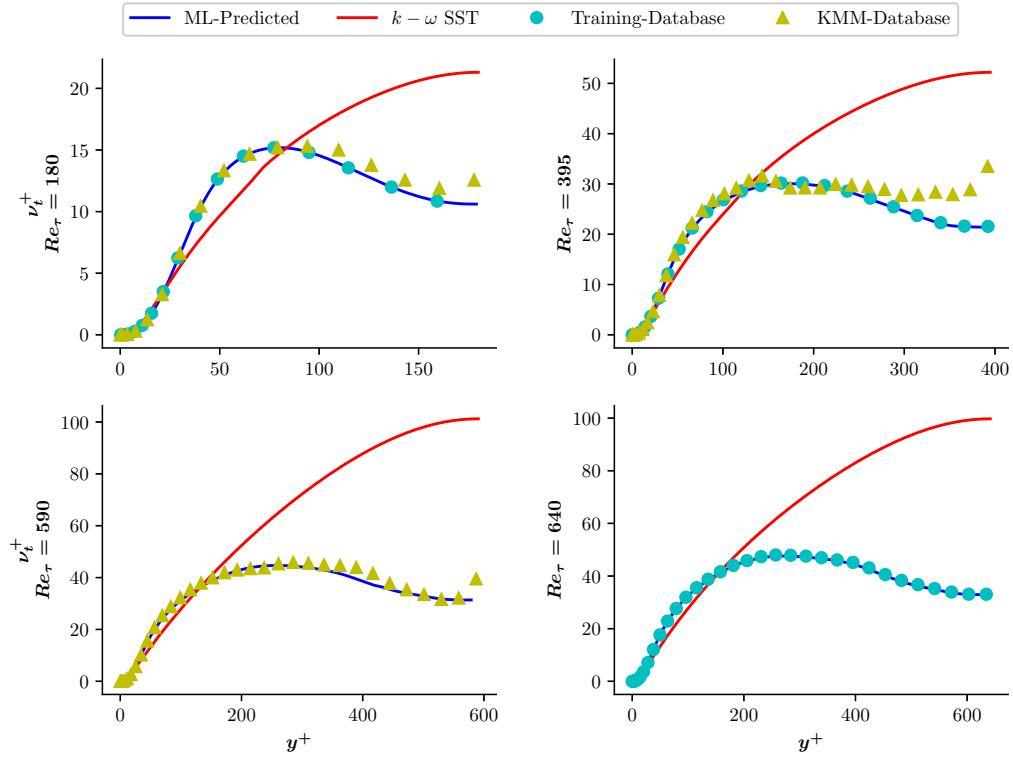


FIG. 10. Comparison of eddy-viscosity distributions along wall normal direction.

of samples for averaging.

According to the posterior results, it can be confirmed that the developed ML-RANS framework can ensure the convergence of a simulation, and for the simulation has the same conditions as the training case, the ML-RANS framework can further ensure the result will converge to the training data. Besides, the posterior results present an nearly zero-error performance from the database used in training process, indicating the presented framework maintains the consistency between priori and posterior results.

To evaluate the robustness and interpolation capability of the developed ML model, we further test the ML-RANS solver in the channel flow at Reynolds number changing continuously from $Re_\tau = 180$ to $Re_\tau = 630$. The profiles of mean velocity and eddy-viscosity are presented in Fig. 11 and Fig. 12 respectively, and the skin friction coefficients are presented in Fig. 13. It can be confirmed that the linear law and log law of the velocity profile are well preserved in all the tests, and the friction coefficients agree well with the law of Dean [49] and the Blasius friction law. From the tested results, we can see a consistent changing of profiles with the Reynolds number, demonstrating a favorable robustness and interpolation capability of the ML model within the range of training data.

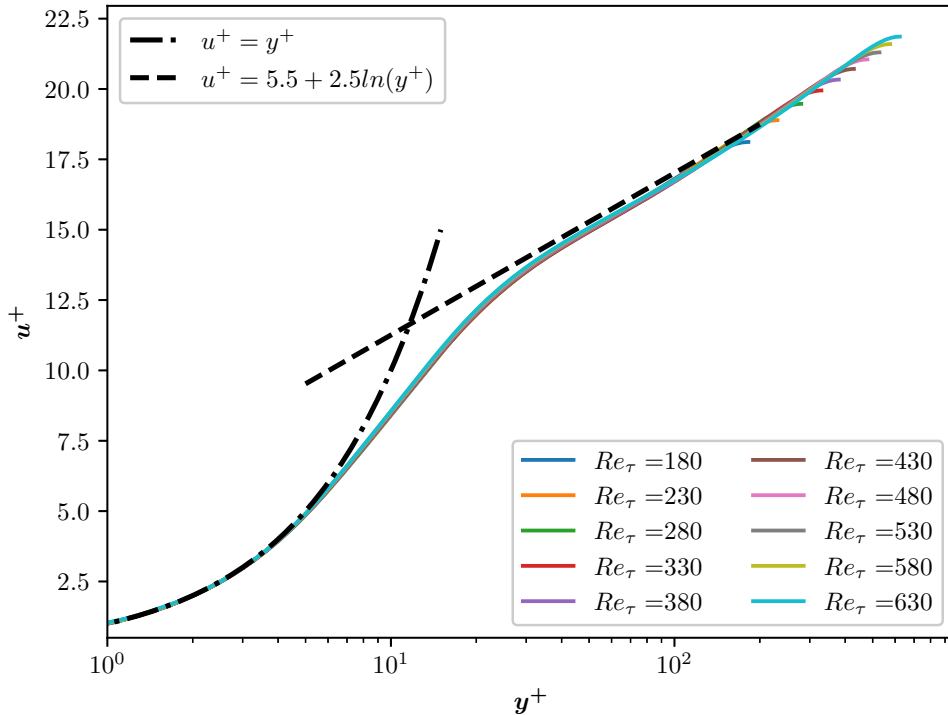


FIG. 11. Mean velocity profiles in channel flows at equally spaced Reynolds numbers.

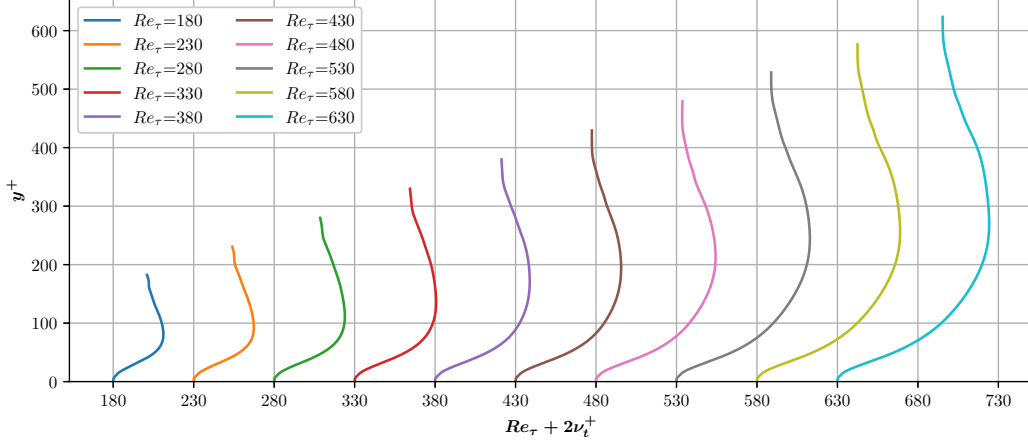


FIG. 12. Distributions of eddy-viscosity in channel flows at equally spaced Reynolds numbers.

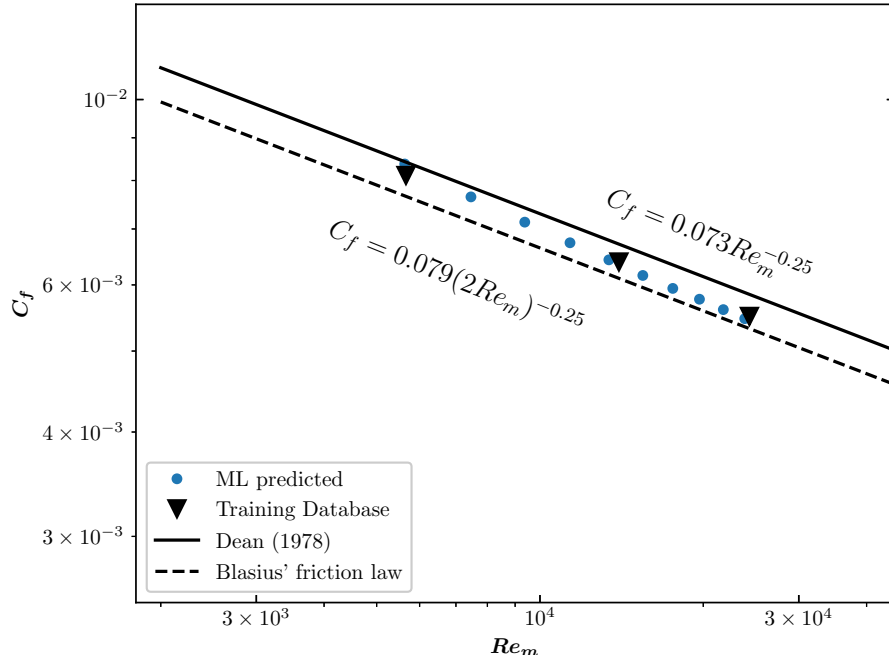


FIG. 13. Comparison of friction coefficients of the ML models prediction, DNS and analytical formula.

To further check the performance of the ML model, the flow over periodic hills at $Re_h = 1400$ is simulated using RANS with both the $k - \omega$ SST model and the ML model trained with data of channel flows. The flow over the periodic hills undergoes a large separation in the downwind side of the hill, posing a great difficulty for RANS model to predict the flow in the separation area [50]. The comparison of the mean velocity fields from DNS, k

- ω SST model, and the ML model is presented in Fig. 14. The ML model, without any training in a flow with a separation, presents a better result than the original $k - \omega$ SST model. The reattachment point and the length of the separation bubble are closer to the DNS results. The streamwise velocity profiles also demonstrated an improvement against the $k - \omega$ SST model, as shown in Fig. 15. The comparison of mean skin friction coefficients and pressure coefficient on the bottom wall further proved the better performance of ML model, as shown in Fig. 16. The positive improvement indicates that the ML model, even trained in simple flow cases, might be able to capture several detailed flow features that is overlooked previously in channels. And such features play a more important role in flows with separations.

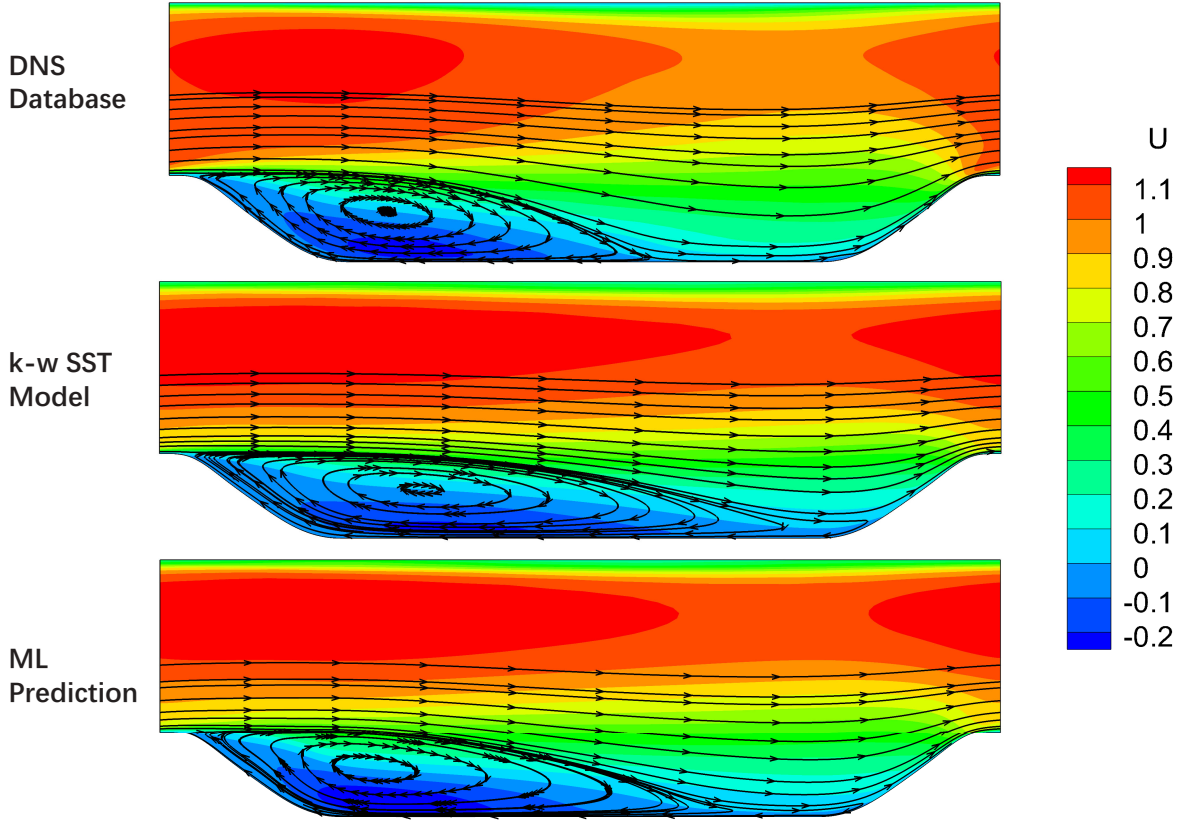


FIG. 14. Mean velocity field in the flow over periodic hills.

The other uncertainty might come from the isotropic nature of eddy-viscosity hypothesis, failing to predict the condition where the principal axis of RS tensor deviates from those of strain rate tensor. However, this results also shows a great potential of the ML model to achieve a favorable prediction in complex flows given enough training from simple cases.

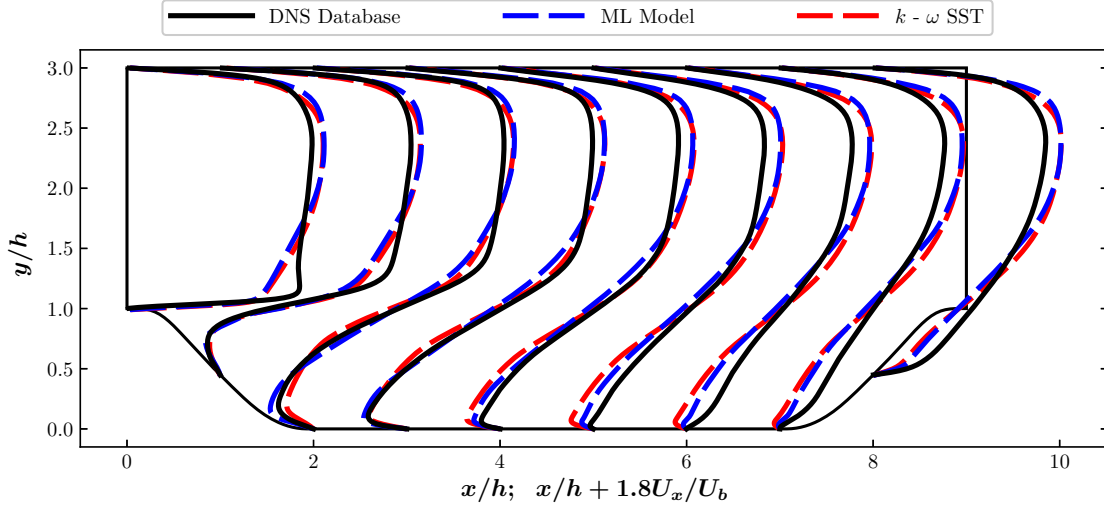


FIG. 15. Comparison of mean streamwise velocity profiles in flow over periodic hills.

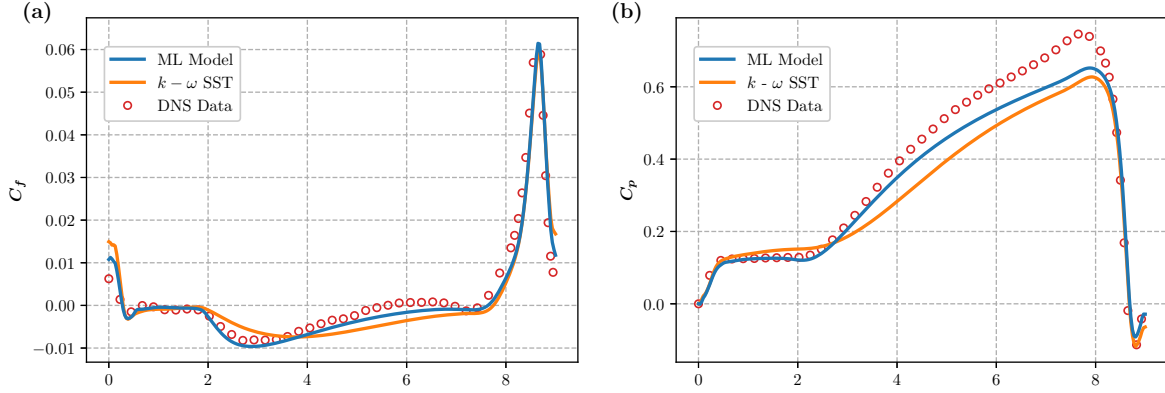


FIG. 16. Distribution of friction coefficient (a) and pressure coefficient (b) on the bottom wall of the periodic hill.

Besides, a trustful prediction is still available when the manifold of data from prediction cases is slightly beyond the training sets.

Therefore, the ML model developed in the present study not only succeeds in the simulation of the same type of flows as the training dataset, but also presents a fairly good result for a more complicated flow beyond the training dataset. This is very encouraging for the further development and applications of the ML model.

V. CONCLUSION

A ML-RANS framework is developed by coupling the Tensorflow and OpenFOAM using a recently developed interface as a platform for the machine-learning based turbulence modelling. The following technical details have been implemented,

1. The Reynolds stress tensor is decomposed into the linear part and the residual non-linear part, overcoming the ill-conditioned problem of RANS equations when utilizing data from high-fidelity simulations.
2. The existing constitutive hypothesis are extended with more variables to ensure the sufficiency of the independent variable.
3. A conventional RANS model (the $k - \omega$ SST model is used for the present case) is incorporated to supply an empirical estimation of turbulent quantities.
4. The convergence of the RANS solver in the prediction phase is ensured for all test cases.

The developed ML-RANS framework is trained in the turbulent channel flows at $Re_\tau = 180, 395, 640$, and tested in channel flows at Reynolds numbers equally spaced within the training range and a flow over periodic hills. The results show that the ML model gives accurate results in the channel flow for both mean velocity and high-order statistics. For the test case of the flow over periodic hills, the solver also presents a fairly better result than the $k - \omega$ SST model although no any priori information about the non-equilibrium flow has been input to the ML model. This indicates the very promising future of the data-driven turbulence modeling.

In spite of $k - \omega$ SST model being incorporated in the current ML model, all the existing turbulence model could be used to provide a proper estimation of turbulence quantities to assist the ML model. In this sense, the developed ML-RANS framework can be regarded as the combination of the data driven turbulence modelling and the traditional turbulence modelling. It should be mentioned that the training data in this case is carefully selected for its good quality. When applying data from complex flows, the data could be noisy due to both the numerical issues of the training dataset and ML modelling process. Therefore, a proper way of processing training data is needed. Also, further cross-case training should be conducted.

ACKNOWLEDGMENTS

The authors would like to dedicate this paper to Prof. Lipeng Lu, the supervisor of Weishuo Liu and Jian Fang, who has left us in February 2019. He devoted all his life studying the mystery in turbulence flow and modeling, and was always caring everything about his students beyond academic affairs. This work wouldnt have been done without his contribution and academic outlook. His elegance, kindness, demeanor and optimism fighting against fatal illness will long be remembered by us.

The project is supported by the National Natural Science Foundation of China (Grant Nos. 51420105008). Dr. Fang gratefully acknowledges financial support from EPSRC under Grant Nos. EP/L000261/1 and EP/K024574/1.

-
- [1] J. Slotnick, A. Khodadoust, J. Alonso, D. Darmofal, W. Gropp, E. Lurie, and D. Mavriplis, *CFD vision 2030 study: a path to revolutionary computational aerosciences*, Tech. Rep. (2014).
 - [2] M. M. Rogers, *Progress Towards the CFD Vision 2030*, Tech. Rep. (2018).
 - [3] B. E. Launder, G. J. Reece, and W. Rodi, Progress in the development of a reynolds-stress turbulence closure, *Journal of fluid mechanics* **68**, 537 (1975).
 - [4] B. E. Launder and B. Sharma, Application of the energy-dissipation model of turbulence to the calculation of flow near a spinning disc, *Letters in heat and mass transfer* **1**, 131 (1974).
 - [5] F. R. Menter, Two-equation eddy-viscosity turbulence models for engineering applications, *AIAA Journal* **32**, 1598 (1994).
 - [6] F. R. Menter, M. Kuntz, and R. Langtry, Ten years of industrial experience with the sst turbulence model, *Turbulence, heat and mass transfer* **4**, 625 (2003).
 - [7] P. Spalart and S. Allmaras, A one-equation turbulence model for aerodynamic flows, in *30th aerospace sciences meeting and exhibit*, p. 439.
 - [8] S. Wallin and A. Johansson, An explicit algebraic reynolds stress model for incompressible and compressible turbulent flows, *Journal of Fluid Mechanics* **403**, 89 (2000).
 - [9] D. C. Wilcox, Formulation of the k-w turbulence model revisited, *AIAA Journal* **46**, 2823 (2008).
 - [10] D. C. Wilcox, *Turbulence modeling for CFD*, Vol. 2 (DCW industries La Canada, CA, 1998).

- [11] S. Kline, B. Cantwell, and G. Lilley, Complex turbulent shear flows: comparison of computation and experiment, Thermosciences Division, Mech. Engg. Dept., Stanford (1982).
- [12] Y. Liu, X. Yu, and B. Liu, Turbulence models assessment for large-scale tip vortices in an axial compressor rotor, *Journal of Propulsion and Power* **24**, 15 (2008).
- [13] F. Villalpando, M. Reggio, and A. Ilinca, Assessment of turbulence models for flow simulation around a wind turbine airfoil, *Modelling and simulation in Engineering* **2011**, 6 (2011).
- [14] C. J. Roy and F. G. Blottner, Review and assessment of turbulence models for hypersonic flows, *Progress in Aerospace Sciences* **42**, 469 (2006).
- [15] D. Michie, D. J. Spiegelhalter, and C. Taylor, Machine learning, Neural and Statistical Classification **13** (1994).
- [16] K. Duraisamy, G. Iaccarino, and H. Xiao, Turbulence modeling in the age of data, *Annual Review of Fluid Mechanics* **51**, 357 (2019).
- [17] J. N. Kutz, Deep learning in fluid dynamics, *Journal of Fluid Mechanics* **814**, 14 (2017).
- [18] P. A. Durbin, Some recent developments in turbulence closure modeling, *Annual Review of Fluid Mechanics* **50**, 77 (2018).
- [19] E. J. Parish and K. Duraisamy, A paradigm for data-driven predictive modeling using field inversion and machine learning, *Journal of Computational Physics* **305**, 758 (2016).
- [20] J. R. Holland, J. D. Baeder, and K. Duraisamy, Towards integrated field inversion and machine learning with embedded neural networks for rans modeling, in *AIAA Scitech 2019 Forum* (2019) p. 1884.
- [21] A. P. Singh, S. Medida, and K. Duraisamy, Machine-learning-augmented predictive modeling of turbulent separated flows over airfoils, *AIAA Journal* , 2215 (2017).
- [22] K. Duraisamy, Z. J. Zhang, and A. P. Singh, New approaches in turbulence and transition modeling using data-driven techniques, in *53rd AIAA Aerospace Sciences Meeting*, <https://arc.aiaa.org/doi/pdf/10.2514/6.2015-1284>.
- [23] B. D. Tracey, K. Duraisamy, and J. J. Alonso, A machine learning strategy to assist turbulence model development, in *53rd AIAA Aerospace Sciences Meeting*, <https://arc.aiaa.org/doi/pdf/10.2514/6.2015-1287>.
- [24] K. Duraisamy and P. Durbin, Transition modeling using data driven approaches, in *CTR Summer Program* (2014) p. 427.
- [25] J. Ling, A. Kurzawski, and J. Templeton, Reynolds averaged turbulence modelling using deep

- neural networks with embedded invariance, *Journal of Fluid Mechanics* **807**, 155 (2016).
- [26] S. B. Pope, A more general effective-viscosity hypothesis, *Journal of Fluid Mechanics* **72**, 331340 (1975).
- [27] J. Ling, R. Jones, and J. Templeton, Machine learning strategies for systems with invariance properties, *Journal of Computational Physics* **318**, 22 (2016).
- [28] J.-X. Wang, J.-L. Wu, and H. Xiao, Physics-informed machine learning approach for reconstructing reynolds stress modeling discrepancies based on dns data, *Physical Review Fluids* **2**, 034603 (2017).
- [29] J.-L. Wu, H. Xiao, and E. Paterson, Physics-informed machine learning approach for augmenting turbulence models: A comprehensive framework, *Physical Review Fluids* **3**, 074602 (2018).
- [30] J. Weatheritt and R. Sandberg, A novel evolutionary algorithm applied to algebraic modifications of the rans stressstrain relationship, *Journal of Computational Physics* **325**, 22 (2016).
- [31] J. Weatheritt and R. Sandberg, The development of algebraic stress models using a novel evolutionary algorithm, *International Journal of Heat and Fluid Flow* **68**, 298 (2017).
- [32] H. Akolekar, J. Weatheritt, N. Hutchins, R. Sandberg, G. Laskowski, and V. Michelassi, Development and use of machine-learnt algebraic reynolds stress models for enhanced prediction of wake mixing in low-pressure turbines, *Journal of Turbomachinery* **141**, 041010 (2019).
- [33] J. Wu, H. Xiao, R. Sun, and Q. Wang, Reynolds-averaged navierstokes equations with explicit data-driven reynolds stress closure can be ill-conditioned, *Journal of Fluid Mechanics* **869**, 553 (2019).
- [34] R. L. Thompson, L. E. B. Sampaio, F. A. de Bragana Alves, L. Thais, and G. Mompean, A methodology to evaluate statistical errors in dns data of plane channel flows, *Computers & Fluids* **130**, 1 (2016).
- [35] W. Rodi, A new algebraic relation for calculating the reynolds stresses, in *Gesellschaft Angewandte Mathematik und Mechanik Workshop Paris France*, Vol. 56.
- [36] H. Abe, H. Kawamura, and Y. Matsuo, Direct numerical simulation of a fully developed turbulent channel flow with respect to the reynolds number dependence, *Journal of Fluids Engineering* **123**, 382 (2001).
- [37] J. Lumley, Toward a turbulent constitutive relation, *Journal of Fluid Mechanics* **41**, 413 (1970).

- [38] A. J. Spencer and R. S. Rivlin, Further results in the theory of matrix polynomials, *Archive for rational mechanics analysis* **4**, 214 (1959).
- [39] A. J. M. Spencer and R. S. Rivlin, The theory of matrix polynomials and its application to the mechanics of isotropic continua, *Archive for rational mechanics analysis* **2**, 309 (1958).
- [40] T. Durieux, *Exploring the use of artificial neural network based subgrid scale models in a variational multiscale formulation*, Master’s thesis (2015).
- [41] M. Abadi, P. Barham, J. Chen, Z. Chen, A. Davis, J. Dean, M. Devin, S. Ghemawat, G. Irving, and M. Isard, Tensorflow: A system for large-scale machine learning, in *12th Symposium on Operating Systems Design and Implementation*, pp. 265–283.
- [42] T. Chen, M. Li, Y. Li, M. Lin, N. Wang, M. Wang, T. Xiao, B. Xu, C. Zhang, and Z. Zhang, Mxnet: A flexible and efficient machine learning library for heterogeneous distributed systems, *arXiv: Distributed, Parallel, Cluster Computing* (2015).
- [43] Y. Jia, E. Shelhamer, J. Donahue, S. Karayev, J. Long, R. Girshick, S. Guadarrama, and T. Darrell, Caffe: Convolutional architecture for fast feature embedding, *arXiv preprint arXiv:1408.5093* (2014).
- [44] F. Pedregosa, G. Varoquaux, A. Gramfort, V. Michel, B. Thirion, O. Grisel, M. Blondel, P. Prettenhofer, R. Weiss, V. Dubourg, *et al.*, Scikit-learn: Machine learning in python, *Journal of machine learning research* **12**, 2825 (2011).
- [45] H. G. Weller, G. Tabor, H. Jasak, and C. Fureby, A tensorial approach to computational continuum mechanics using object-oriented techniques, *Computers in Physics* **12**, 10.1063/1.168744 (1998).
- [46] P. Balakumar and G. I. Park, Dns/les simulations of separated flows at high reynolds numbers, in *45th AIAA Fluid Dynamics Conference* (2015) p. 2783.
- [47] R. D. Moser, J. Kim, and N. N. Mansour, Direct numerical simulation of turbulent channel flow up to $Re_\tau = 590$, *Physics of fluids* **11**, 943 (1999).
- [48] R. Tibshiranit, Regression shrinkage and selection via the lasso, *Journal of the royal statistical society series b-methodological* **58**, 267 (1996).
- [49] R. B. Dean, Reynolds number dependence of skin friction and other bulk flow variables in two-dimensional rectangular duct flow, *Journal of Fluids Engineering-transactions of The Asme* **100**, 215 (1978).
- [50] S. Jakirlic, *Extended excerpt related to the test case: Flow over a periodical arrangement of*

2D hills, Tech. Rep. (Technische Universitt Darmstadt, 2012).